Analyst

Accepted Manuscript

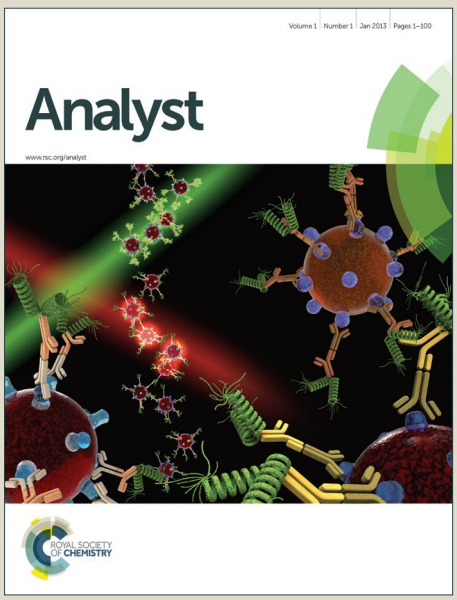

ROYAL SOCIETY OF CHEMISTRY

www.rsc.org/analyst

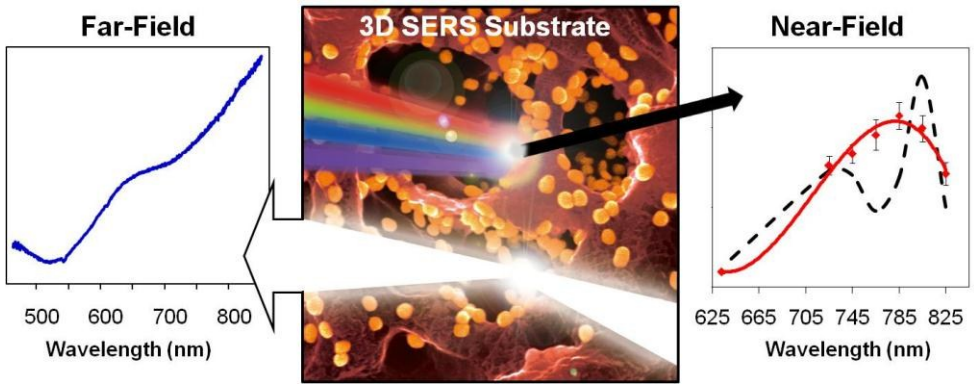

Analyst

ARTICLE

Unraveling Near-Field and Far-Field Relationships for 3D SERS Substrates – A Combined Experimental and Theoretical Analysis

Received 00th January 20xx,
Accepted 00th January 20xx

DOI: 10.1039/x0xx00000x

www.rsc.org/

Dmitry Kurouski,[a,#] Nicolas Large,[a,#] Naihao Chiang,[a,b] Nathan Greeneltch,[a] Keith T. Carron,[c,d] Tamar Seideman,[a,b] George C. Schatz,[a,b] and Richard P. Van Duyne[a,b]*

Simplicity and low cost has positioned inkjet paper- and fabric-based 3D substrates as two of the most commonly used surface-enhanced Raman spectroscopy (SERS) platforms for the detection and the identification of chemical and biological analytes down to the nanogram and femtogram levels. The relationship between far-field and near-field properties of these 3D SERS platforms remains poorly understood and warrants more detailed characterization. Here, we investigate the extremely weak optical scattering observed from commercial and home-fabricated paper-, as well as fabric-based 3D SERS substrates. Using wavelength scanned surface-enhanced Raman excitation spectroscopy (WS-SERES) and finite-difference time-domain (FDTD) calculations we were able to determine their near-field SERS properties and correlate them with morphological and far-field properties. It was found that nanoparticle dimers, trimers, and higher order nanoparticle clusters primarily determine the near-field properties of these substrates. At the same time, the far-field response of 3D SERS substrates either originates primarily from the monomers or cannot be clearly defined. Using FDTD we demonstrate that LSPR bands of nanoparticle aggregates near perfectly overlap with the maxima of the near-field surface-enhanced Raman scattering responses of the 3D SERS substrates. This behavior of far-field spectroscopic properties and near-field surface-enhanced Raman scattering has not been previously observed for 2D SERS substrates, known as nanorod arrays. The combination of these analytical approaches provides a full spectroscopic characterization of 3D SERS substrates, while FDTD simulation can be used to design new 3D SERS substrates with tailored spectral characteristics.

Introduction

Surface-enhanced Raman spectroscopy (SERS) is a valuable analytic technique that allows for detecting molecular analytes down to the single molecule level. After the first demonstration in 1977 that roughness of the noble metal surfaces could drastically amplify the Raman cross-section of molecules absorbed on the substrate or in its viscinity,[1] a wide variety of SERS substrates have appeared.[2-4] The discovery of this surface-enhanced Raman scattering effect suggested an electromagnetic enhancement, which involves localization and amplification of an incident light by surface plasmon resonances(localized and propagating) of noble metals, to be responsible for the high amplification of the Raman signal.[5-8]Localized surface plasmon resonances (LSPRs) are coherent, collective oscillations of the conduction electron gas sustained by noble metal nanoparticles. They are responsible for drastic enhancement of the local electric field (**E**) in the vicinity of the metallic nanoparticle, which can reach 100–1,000 times the incident electric field ($\mathbf{E}_0$). The LSPR strongly depends on nanoparticle size, shape, material, and local dielectric environment.[9-12] On the other hand, propagating surface plasmons (SPPs) are rather typical in noble metal films and generally generate much smaller field enhancements. Numerous SERS platforms have been proposed to achieve the maximization of electromagnetic enhancement such as metal film over nanospheres (FON),[13, 14] colloidal crystals films,[15] nanoparticle arrays,[16-18] particles grafted on silanized glasses,[19] and plasmonic nanoholes.[20-23] Based on the fabrication techniques used, there are several types of SERS platforms. Lithographic substrates are characterized by well-defined nanostructures at specific locations on the substrate and hence to achieve high SERS enhancement factors (typically, 10^6–10^8).[4, 24, 25] One of the most well-developed types of lithographic substrates is periodic particle arrays, which are fabricated by metal evaporation on a mask of close-packed silica or polystyrene spheres.[13, 14, 25] The resulting surface is referred to as metal FON. An alternative method, electron beam lithography (EBL) is commonly used to fabricate arrays with various shapes with tunable interparticle distances.[26, 27] However, high labor intensity and time consumption of EBL-based substrates and high fabrication

[a] Department of Chemistry, Northwestern University, 2145 Sheridan Road, Evanston, IL 60208, USA. Email: vanduyne@northwestern.edu.
[b] Applied Physics Program, Northwestern University, 2145 Sheridan Road, Evanston, IL 60208, USA.
[c] Chemistry Department, University of Wyoming, 1000 East University Avenue, Laramie, WY 82071, USA.
[d] Snowy Range Instruments, 407 S. Second, Laramie, WY, 82070, USA.

† # These authors contributed equally. Electronic Supplementary Information (ESI) available: Figure S1: Reflectance spectra in the range 800-2,000 nm; Figure S2: Calculated absorption spectra of Au nanoparticles in solution. Figure S3: Calculated scattering and integrated near-field spectra of NCAuNR. See DOI: 10.1039/x0xx00000x

costs limit their broad and large scale utilization.[4] The fabrication of non-lithographic substrates is commonly carried out through a thermal evaporation of plasmonic metals on a glass or silicon substrate.[28] It results in generation of nanometer-scale plasmonic features.[29, 30] Although the fabrication of non-lithographic substrates, such as metal islands or porous films, is relatively facile, it is practically impossible to control the nanostructure geometry and architecture and consequently their uniformity.

Chemically synthesized nanoparticles, both in solution and on supports, have been broadly used as alternative SERS substrates. Advantages of this choice include, but are not limited to: high enhancement factors, easy synthesis, and possibility to tailor their sizes and geometries to fulfill the particular experimental needs.[2, 21, 22, 31, 32] Recently, numerous different kinds of nanoparticles have been reported, including porous nanoparticles, octopods/nanostars, octahedra, concaved- and etched nanocubes, and nanocuboids.[21-23, 33-35]However, a large-scale fabrication of nanoparticles is often difficult to achieve. Also, precursors of their synthesis, such as cetyltrimethylammonium bromide (CTAB) and citric acid, commonly overcomplicate their practical applications in surface-enhanced spectroscopies and sensing.[36, 37] Removal of these surfactants commonly leads to random aggregation and precipitation of the metallic nanoparticles, which does not allow for achieving strong reproducibility of the provided SERS enhancement. To overcome this issue, different strategies have been developed to controllably assemble nanoparticles, ranging from simple modulation of electrostatic interactions between colloids to functionalization of nanoparticles with DNA and small organic molecules.[38-40]

An alternative substrate fabrication approach was proposed in 1980s[41-43] and recently commercialized,[44, 45] in which paper or fabric is used to anchor and assemble nanoparticles. These SERS substrates have been demonstrated to be very promising platforms for the detection and identification of various chemical and biological analytes, providing detection down to the nanogram and femtogram levels.[44] It was demonstrated that nanoparticles can be deposited on the substrates using simple ink-jet printers, which drastically decreases their production costs and enables on-site fabrication.[44, 46, 47] During this process, nanoparticles penetrate down through the paper or fabric fibers forming different aggregates on their surfaces. Therefore, these substrates can be considered as the first 3D SERS platforms. Consequently, in the last decade, 3D SERS substrates gained enormous popularity in various fields ranging from analytical chemistry to biology.[31, 48-50] Nevertheless, the lack of detailed fundamental studies of their spectroscopic properties limits our understanding about their functionality and subsequent design of new 3D SERS substrates with tailored optical properties.

In this manuscript we performed a comprehensive spectroscopic characterization and microscopic examination of three different 3D SERS substrates (two are commercial). It is found that the optical scattering from these substrates has only a weak wavelength dependence, which prevents us from resolving or identifying their LSPR modes. However, significant insights may be derived from wavelength scanned surface-enhanced Raman excitation spectroscopy (WS-SERES), which is a sophisticated spectroscopic approach that was previously demonstrated to successfully characterize the near-field response of SERS substrates and aggregated nanoparticles.[51]The WS-SERES results obtained for the 3D SERS substrates are correlated with their morphological properties as obtained by scanning electron microscopy (SEM). This shows that the size, aggregation state and density coverage of gold nanoparticles (AuNPs) have very little correlation with the enhancement and near-field SERS properties of these 3D SERS platforms. Based on the experimental near-field responses of the 3D SERS substrates and their microscopic investigation by finite-difference time-domain (FDTD) calculations, we have determined the LSPR profiles of the 3D SERS substrates, and this allows us to define a relationship between far-field spectroscopic properties and near-field surface-enhanced Raman scattering. The resulting theoretical models can be used to design new 3D SERS substrates with desired spectral characteristics.

Experimental

Materials. The commercial spherical AuNP 3D SERS substrates were generously provided by iFyber LLC (Ithaca, NY, USA) and AnSERS (College Park, MD, USA). The non-commercial gold nanorod (AuNR) 3D SERS substrates were fabricated by Rabolt and co-workers (University of Delaware, Newark, DE).[52] For the sake of simplicity, AuNP 3D SERS substrates received form iFyber LLC and AnSERS are named 'IFAuNP' and 'ANAuNP', respectively. The non-commercial AuNR 3D SERS substrates are named 'NCAuNR'. Detailed procedures of substrate manufacturing have been published elsewhere.[31, 44-46, 50, 52] All substrates were used as received, without further treatment and functionalization.

Benzenethiol (Sigma-Aldrich, St. Louis, MO, USA) was vapor-deposited onto the substrates by placing 3–4 drops of concentrated (100%) benzenethiol solution in a Petri dish around the substrate. Substrates were left overnight in the atmosphere of benzenethiol vapors and measured using WS-SERES immediately after.

Cyclohexane (Sigma-Aldrich, St. Louis, MO, USA) was used as an intensity standard (1028.3 cm^{-1} normal Raman scattering band) for a correction of the inherent v^4 behavior of Raman scattering. Specifically, the intensity of the 1075 cm^{-1} band of benzenethiol, which was used as a reported of SERS signal for all 3D substrates, was divided by the intensity of the 1028.3 cm^{-1} band of cyclohexane to obtain the SERS efficiency at each excitation wavelength. Such normalization also allow us to eliminate variations in the SERS intensity that are not due to enhancement by the substrate, as well as the spectral dependence of the detection system.[51]

Raman Spectroscopy. SERS and normal Raman spectra were collected on an inverted microscope (Nikon TE-300) with 20Xdry Nikon objective (NA=0.45). A diode pumped solid-state laser

Spectra-Physics (Mountain View, CA, USA) Millenia Xs was used for 532 nm excitation. It was also used to drive the tunable Ti:Sapphire oscillator to generate wavelengths from 725 to 825 nm. Spectra-Physics He-Ne diode-based laser was used to generate a 633 nm laser excitation. The signal was collected in a backscattering configuration and directed to a confocal Raman spectrometer (Princeton Instruments, SP2500i) equipped with a 1200 groove/mm grating blazed at 500 nm (532 nm excitation) or 600 groove/mm grating blazed at 750 nm (633, 725–825 nm excitation) and a slit entrance set to 100 µm. Prior to entering the spectrograph Rayleigh scattering was filtered with a long-pass filter (Semrock, LP03–532RS-25 (532 nm excitation) or LP03–633RS-25 (633 nm excitation)). To filter the Rayleigh scattering at 725–825 nm excitations, a 900/11 nm VersaChrome tunable band-pass filter was used. The dispersed light was then sent to a liquid nitrogen-cooled CCD (Action300i, Spec-10 400B). A motorized stage (Physik Instrumente, 710 Digital PZT) was used to move the sample relative to the incident laser beam. All data was processed using GRAMS/AI 7.0 (Thermo Galactic, Salem, NH).

UV-Vis Spectroscopy. Scattering spectra (400–900 nm) were recorded by illuminating the sample with the microscope lamp and analyzing the transmitted light by a fiber-optically coupled Ocean Optics spectrometer (SD200, Ocean Optics, Dundein, FL, USA).[25] T_{aqu}=10 ms and 103 averages. Uncoated fabric of the corresponding substrate was used as a reference to reach 100% transmission. Scattering spectra within 900–2,000 nm were recorded using Agilent Cary 5000 UV/Vis/NIR spectrometer with Agilent Internal DRA 2500 UV/vis/NIR (InGaAs) Module.

Scanning Electron Microscopy. SEM images were taken at Hitachi SU8030 using a 10 kV acceleration voltage. Prior to imaging substrates were coated with 9 nm of osmium using osmium plasma coater to enrich their conductivity.

Results and discussion

Microscopic Examination

We performed SEM imaging to investigate morphological organization of the IFAuNP, ANAuNP, and NCAuNR 3D SERS substrates (Figure 1). One can notice that IFAuNP, ANAuNP, and NCAuNR 3D SERS substrates have different textures. The IFAuNP substrate is very dense and porous with AuNPs average size of 90 nm adsorbed on the surface of the fabric polymer. These AuNPs form small clusters (*e.g.,* dimers, trimers, and quadrumers) of different arrangements in addition to single, isolated nanoparticles (Figure 1, red). The ANAuNP substrate appears to be much less

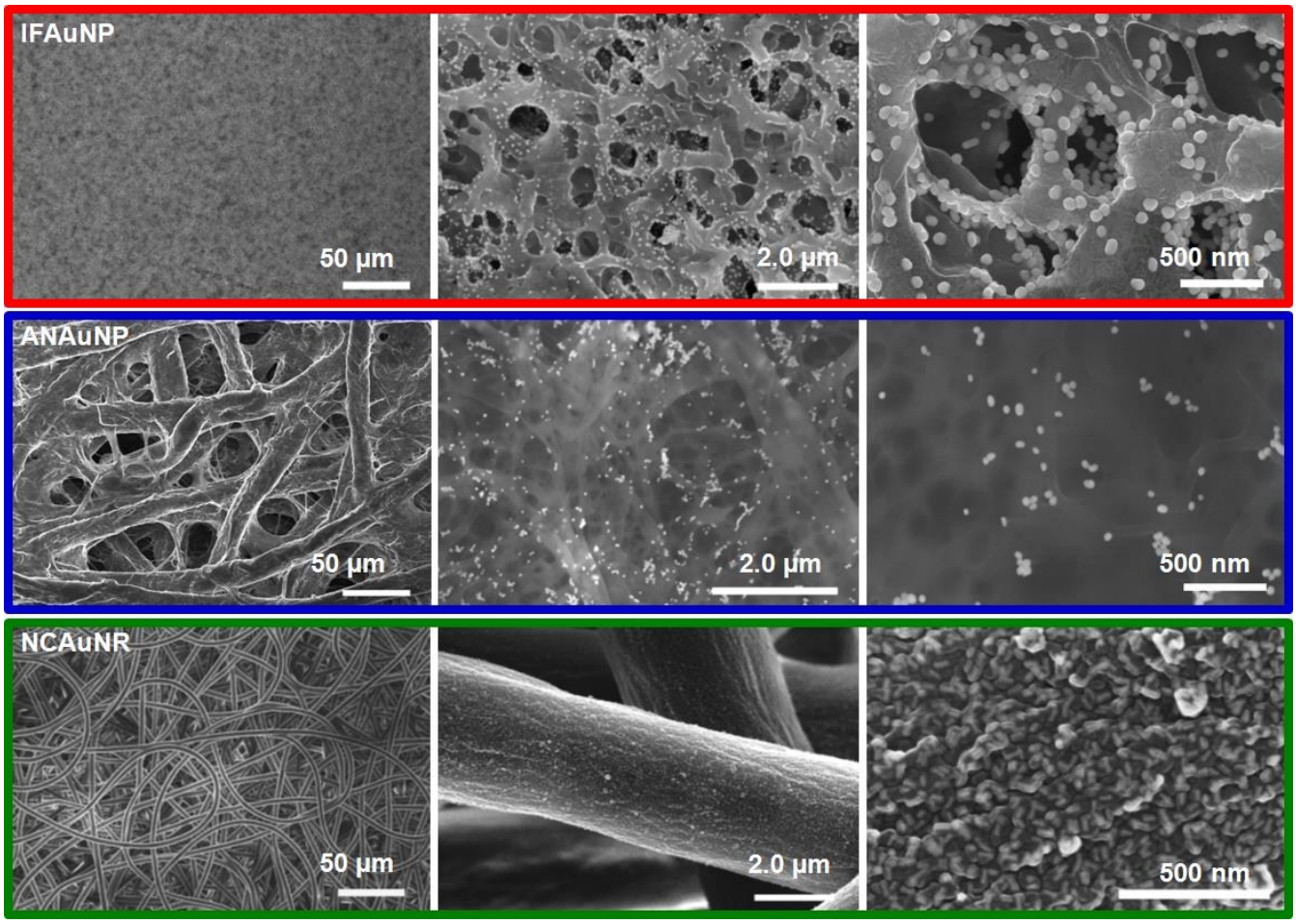

Figure 1. SEM images of IFAuNP (top row, red), ANAuNP (middle row, blue), and NCAuNR (bottom row, green) 3D SERS substrates at different magnifications.

dense than IFAuNP and has a clearly visual fiber structure (Figure 1, blue). The density of the 50 nm AuNPs is found to be much lower than that of IFAuNP. Nevertheless, similarly to the IFAuNP substrate the AuNPs are organized in small isolated clusters. Finally, the NCAuNR 3D SERS substrate is composed of a web of fibers with a diameter of around 3–4 μm (Figure 1, green). The surface of these individual fibers is densely covered by AuNRs that are about 50 nm in length and 10 nm in width.

Far-Field Scattering

Far-field scattering spectra are commonly used to predict the near-field properties of metallic nanoparticles and guide the rational design of SERS substrates. We have investigated far-field scattering properties of 3D SERS substrates by illuminating their surface with a white light source. The reflected radiation was collected in a backscattering configuration. The corresponding blank fabric substrate without deposited AuNPs or AuNRs was used as a reference (100% reflectance). Surprisingly, all three substrates, IFAuNP, ANAuNP, and NCAuNR, exhibited very similar features in their spectra profiles (Figure 2A).

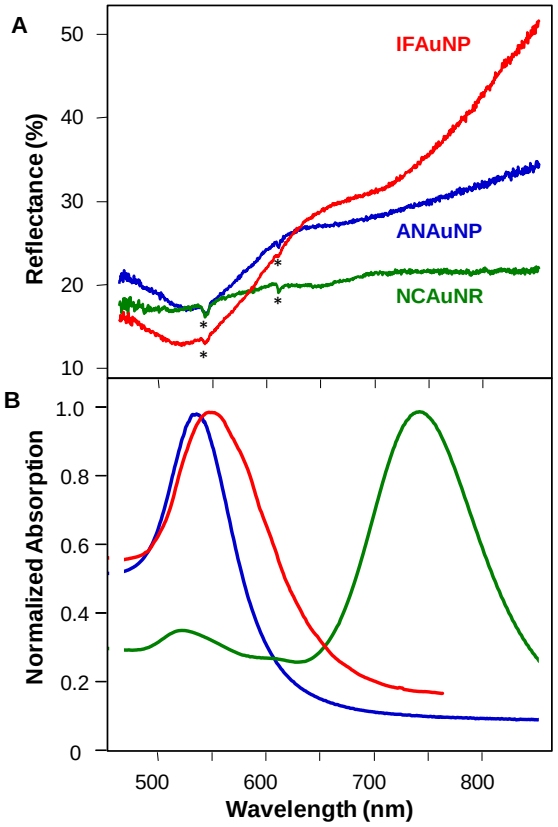

Figure 2. (A) Reflectance spectra of IFAuNP (red), ANAuNP (blue), and NCAuNR (green) 3D SERS substrates. (B) Absorption spectra in solution of AuNPs and AuNRs used in the fabrication of the three SERS substrates (red: 90 nm nanospheres, blue: 50 nm nanospheres, and green: 10×50 nm nanorods). Spectrometer artefacts are marked with asterisks (*) in panel A.

Spectra measured from IFAuNP (red line) and ANAuNP (blue line) substrates showed a gradual decrease in the reflectance with decreasing wavelengths, exhibiting a minimum at ~550 nm and a weak feature around 700 nm. NCAuNR substrate (green line) exhibits a relatively flat reflectance spectrum in the range 500–800 nm. It should be noticed that IFAuNP and ANAuNP substrates have a visual dark-red color, while NCAuNR substrate is dark-purple, and therefore should exhibit a LSPR in the visible spectral range.

To gain more insight in the optical properties of these substrates, we looked at the far-field response of colloidal solutions of the AuNPs and AuNRs used to fabricate these 3D SERS substrates (Figure 2B). The absorption spectra of AuNPs (red and blue lines) exhibit the typical spectra for spherical monomers with a dipolar LSPR mode at ~550 nm. These nanosphere optical spectra are in excellent agreement with results from Mie theory (Supporting Information, Figure S2), thus showing the high quality and uniformity of the AuNPs in the analyzed solutions. Consequently, from all aggregation states of the AuNPs on both IFAuNP and ANAuNP substrates, monomers (band at ~550 nm) should primarily contribute to the optical responses of these substrates. At the same time, it was previously demonstrated that individual AuNPs exhibit no SERS due to very small EF ($\leq 10^4$).[53] Indeed, both IFAuNP and ANAuNP do not show a SERS enhancement at 532 nm excitation (data not shown). A barely noticeable LSPR band at ~700 nm in the optical scattering spectra of IFAuNP and ANAuNP is not visible in the absorption spectra of corresponding AuNP solutions. It was previously reported that aggregation of nanoparticles, which takes place upon their deposition on the paper or fabric substrate, results in a spectral red-shift of their LSPR.[54, 55] Therefore, LSPR band at ~700nm can be assigned to different aggregation states of AuNPs (dimers, trimers, and their higher order clusters).

The absorption spectrum of AuNRs exhibits two distinct peaks at ~550 nm and at ~750 nm for the AuNRs (Figure 2B, green line), corresponding to the transverse and longitudinal dipolar LSPR, respectively. However, optical response of NCAuNR substrate did not reveal any LSPR of individual NRs or from their aggregates in the ranges 400–900 nm and 900–2,000 nm (Supporting Information, Figure S1). These results indicate that the near-field properties of IFAuNP, ANAuNP, and NCAuNR 3D SERS substrates, and consequently the spectral region in which they would provide the highest SERS enhancement, could not be clearly predicted based on a direct measurement of their far-field response.

Near-Field SERES Response

We used WS-SERES to investigate the near-field response of IFAuNP, ANAuNP, and NCAuNR 3D SERS substrates. This analytic technique has previously been used with success to characterize the near-field SERS response of non-lithographic 2D nanoparticle arrays,[51] lithography-based nanorod arrays,[16] and double-core nanoantennas.[56] The results reported in the literature generally support the strong correlation between near-field SERS enhancement and far-field Rayleigh scattering, although exceptions can arise.[56]

Several individual IFAuNP, ANAuNP, and NCAuNR substrates were examined using WS-SERES by measuring the near-field SERS response from 6–9 different, non-overlapping spots on each sample. The excitation wavelengths employed in all the measurements were 532, 633, 725, 735, 745, 755, 765, 775, 785, 795, 805, 815, and 825 nm. Representative SERS spectra of benzenethiol acquired on IFAuNP, ANAuNP, and NCAuNR 3D SERS substrates are shown in Figure 3. All bands exhibited the same relative SERES profile shape, therefore the intensity of benzenethiol peak at 1075 cm^{-1} was used to plot SERES efficiency profiles of IFAuNP, ANAuNP, and NCAuNR 3D SERS substrates (Figure 4).

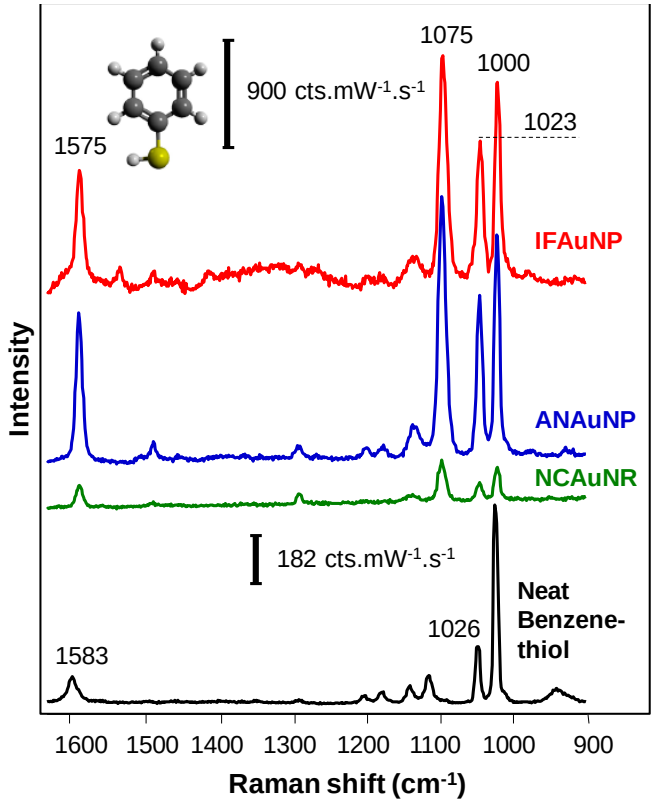

Figure 3. SERS spectra of benzenethiol (inset) acquired on IFAuNP (red), ANAuNP (blue), and NCAuNR (green) 3D SERS substrates. λ=785 nm, *P*=103 μW, and *T*=10 s. Normal Raman spectrum of neat benzenethiol obtained at λ=785 nm, *P*=2.5 mW, and *T*=1 s.

SERES measurements reveal that IFAuNP and ANAuNP 3D SERS substrates have similar SERS efficiencies (Figure 4A, B). The Gaussian profiles obtained for IFAuNP and ANAuNP exhibit their maxima around 765–805 and 745–825 nm, respectively. Both substrates show a SERS efficiency of ~10% at 633 nm and of 0% at 532 nm (data not shown). Notice that ANAuNP demonstrates a large SERS efficiency over a broader spectral range than the IFAuNP substrate, associated with the formation of small AuNP clusters of different size and arrangements (Figure 1, blue). It should be noted that AuNPs with different sizes (*d*=90 and 50 nm) were used for the fabrication of these 3D SERS substrates (IFAuNP and ANAuNP, respectively). AuNPs density and their aggregation state were also found different on both IFAuNP and ANAuNP (Figure 1). Nevertheless, WS-SERES reveals nearly identical enhancement efficiency at ~785 nm for both of these substrates (Figure 4). This indicates that size, aggregation state, and density coverage of AuNP have negligible effects on the enhancement efficiency and near-field SERS properties of these 3D SERS platforms.

The SERES profile of NCAuNR substrates is substantially different than that of IFAuNP and ANAuNP. It exhibits an exponential increase of the SERS efficiency from 633 to 825 nm, suggesting that the SERS efficiency maximum would be observed in the near-infrared (≥825 nm). However, due to instrumental limitations, we are unable to measure WS-SERES profiles in this spectral region. It should be noted that from 633 to 825 nm NCAuNR exhibit 100 times less SERS efficiency than IFAuNP and ANAuNP. Similarly to these commercial substrates, NCAuNR does not provide SERS enhancement at 532 nm (data not shown).

Electrodynamic Modeling of Near-field Response

To interpret these results we performed FDTD simulations (Lumerical FDTD Solutions)[57] to calculate the plasmonic properties (far- and near-field) of the IFAuNP, ANAuNP, and NCAuNR substrates. Using the SEM structures in Figure 1, we have modeled the IFAuNP and ANAuNP substrates as randomly distributed spherical AuNPs of diameter *a*=90 and 50 nm, respectively. The modeled NCAuNR substrate is taken to be ellipsoidal AuNRs of length *L*=50 nm and width *l*=10 nm. The dielectric permittivity tabulated by Johnson and Christy has been used for gold.[58] The cellulose-based polymers supporting the gold nanoparticles in the three SERS substrates are taken as semi-infinite dielectric substrates of refractive index n_s=1.475.[59] To correctly discretize the nanostructure the FDTD mesh size is fixed at 1 nm in all the calculations.

As part of the random generation of the AuNP distributions, distances between AuNPs vary from distribution to distribution. Therefore, the LSPR intensities and positions may significantly vary from distribution to distribution. Consequently it is necessary to average the results over several distributions to account for the heterogeneity of the experimental substrates. The averaged near-field response of AuNPs and AuNRs is determined for particles that are randomly distributed over 1.5×1.5 μm flat surfaces. Periodic boundary conditions are then applied to this simulation domain. The IFAuNP substrate is modeled with uniform distributions of nanoparticles, and the ANAuNP substrate is modeled with uniform distributions of small clusters composed of *N*=1–5 AuNPs. The size and arrangement of these clusters are also randomly, uniformly generated. The nanoparticle surface densities are taken to be $\rho=2.5\times10^{-5}$ nm^{-2} and $\rho=2.0\times10^{-5}$ nm^{-2} for IFAuNP and ANAuNP, respectively. Calculations are performed and averaged over the two in-plane polarizations, and over 5 different nanoparticle (or nanocluster) distributions. Since the NCAuNR substrate exhibits an extremely high density of nanoparticles, random AuNR distributions are generated with different nanorod surface densities ($\rho=2.5\times10^{-4}$ to 2.5×10^{-3} nm^{-2}). Although we do not have access to experimental

values of the nanoparticle densities, the values used in the FDTD calculations are chosen to provide the best agreement with the experimental results; therefore, they can be considered as reasonable estimates of AuNPs and AuNRs densities. The electromagnetic SERS enhancement factor (EF) is given by the fourth power of the near-field, $EF \approx |\mathbf{E}/\mathbf{E}_0|^4$.[60, 61] Calculated EF distributions are shown in Figure 4D-F for the three SERS substrates. In order to compare with the experimental SERS efficiency, we calculate and integrate the fourth power of the near-field (*i.e.,* EF) over the volume of the modeled samples.[21, 22] The integrated near-field enhancements, $\langle |\mathbf{E}/\mathbf{E}_0|^4 \rangle$, normalized to the volume and calculated at the same wavelengths as the experimental SERES profiles, are shown in Figure 4A-C. It is important to notice that the integration domain in FDTD (finite-size unit cell) is far smaller than the experimentally probed volume; therefore the variation in the absolute values of $\langle |\mathbf{E}/\mathbf{E}_0|^4 \rangle$ is greater at low NP density (*e.g.*, ANAuNP and IFAuNP). The spectral position of the maximum enhancement and the decay towards lower wavelengths are in good agreement with the experimental observations. However, there is a large difference in the bandwidth of the calculated enhancement profiles compared to the experimental SERES profiles. This difference is directly related to (i) inhomogeneity of the IFAuNP and ANAuNP substrates, and (ii) the spatial region probed experimentally which is much larger than the distributions used in the FDTD simulations.

Calculated Far-Field Scattering Profiles

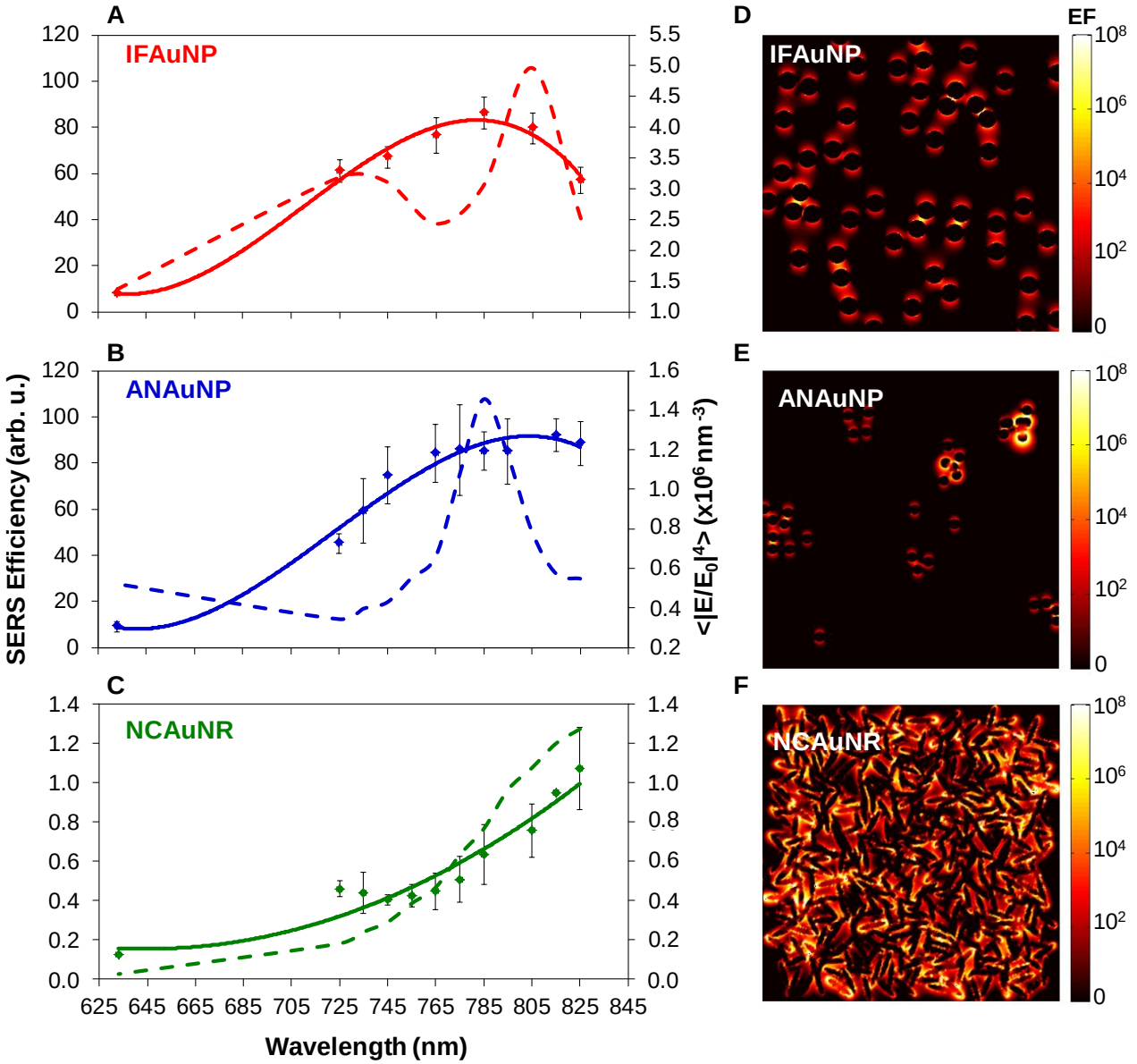

Figure 4. SERES profiles of IFAuNP, ANAuNP, and NCAuNR 3D SERS substrates. The intensity of benzenethiol peak at 1075 cm^{-1} was used as a reference to define the SERS efficiency and the 1028.3 cm^{-1} peak of cyclohexane was used as intensity standard. Data were fitted with a second order polynomial function (solid curves). The spectral dependence of the integrated near-field $\langle |\mathbf{E}/\mathbf{E}_0|^4 \rangle$ calculated using FDTD is plotted (dashed curves) for (A) IFAuNP, (B) ANAuNP, and (C) NCAuNR substrates. The corresponding calculated enhancement factor distributions ($EF \approx |\mathbf{E}/\mathbf{E}_0|^4$), calculated at the maximum value of $\langle |\mathbf{E}/\mathbf{E}_0|^4 \rangle$, are plotted in panels (D-F).

The far-field properties of the IFAuNP, ANAuNP, and NCAuNR SERS substrates have been calculated using FDTD. Similar to the experimentally obtained optical responses, FDTD calculations (Figure 5) clearly show that IFAuNP (red line) exhibits a single, very intense band in the scattering spectrum centered at 550 nm. This intense LSPR, corresponding to the strong dipolar resonance of the individual AuNPs, is expected from the uniform distribution of AuNPs used in this model of the substrate. However, due to the relatively large AuNPs density in this sample, the formation of isolated dimers and trimers in the random distribution is inevitable. The presence of dimers and trimers is not visible in the scattering spectrum (except as a long tail on the long wavelength portion of the red curve); however, these species are easily visible in the near-field (*cf.* Figure 4). Indeed one can notice that the strong SERS enhancement at 800 nm (Figure 4A) is associated with dimer plasmon modes (Figure 4D).

The scattering spectrum of the ANAuNP substrate (blue line) shows two broad bands, at ~550 and ~770 nm, along with a pronounced shoulder at ~845 nm. Similarly to the IFAuNP substrate, the 550 nm LSPR is mainly associated with the dipolar mode of individual AuNPs. The broad band and features observed above 750 nm are associated with plasmon modes formed in the small AuNP clusters (Figure 4E). This plasmon band also correlates with the strong SERS efficiency and integrated near-field observed around ~800 nm (Figure 4B).

Finally, the far-field profile of the NCAuNR substrate (green line) exhibits a gradual increase in scattering from ~600 nm, reaching a plateau around 825 nm. This very broad band observed at high wavelengths originates from the high uniform density of AuNRs.[62] The same trend is observed for the SERS efficiency (Figure 4C), showing that the contribution to the SERS efficiency for this particular substrate originates from multipolar plasmon modes formed by the closely packed AuNRs (Figure 4F).

Interestingly, it appears that the calculated scattering spectra (Figure 5) differ from the experimental far-field profiles obtained from the 3D SERS substrates (Figure 2). These differences are associated with several important factors. First, the 3D nature of the SERS substrate (*cf.* Figure 1), along with the penetration depth of the laser excitation allows for probing more volume (*i.e.,* more AuNPs) into the sample, giving rise to an increase inhomogeneous broadening. It also contributes to the reduction of the collected signal, making more challenging the observation of the low energy plasmon modes observed above 700 nm. Also, contrary to the 2D modeled substrates where the nanoparticles and nanoclusters are only arranged in-plane, the 3D nature of the nanoparticle distributions of the actual substrates allows for more degrees of freedom, thus leading to a larger number of possible plasmon modes excited. Although FDTD calculations would be necessary to confirm these different effects, the complex micron scale superstructures formed by the polymer fibers along with the nanoscale gold nanoparticles randomly distributed at the surface of these fibers make the calculations extremely challenging. In particular, such simulations would require very fine spatial discretization (1–2 nm) over simulation domains of several hundreds of cubic microns, giving rise to simulations that are currently not accessible with the computational resource available. Furthermore, due to the nanoparticle density and arrangements (*i.e.,* interacting nanoparticles) of the three SERS substrates, effective medium theories fail to correctly predict the optical properties of these systems.[63-65]

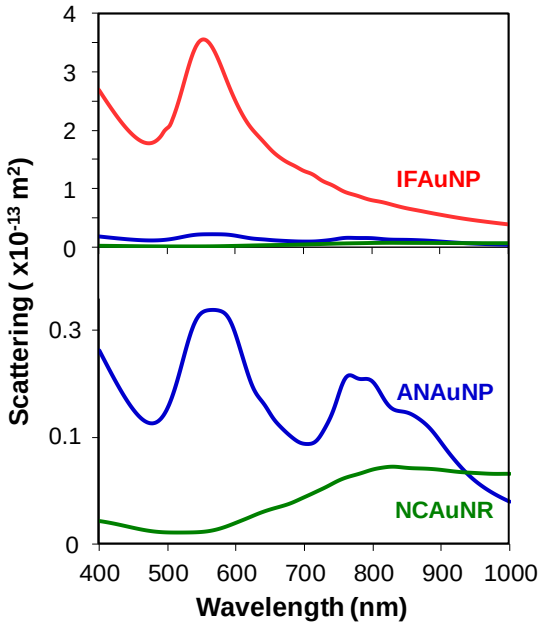

Figure 5. Upper panel: Scattering spectra of IFAuNP (red), ANAuNP (blue), and NCAuNR (green) 3D SERS substrates calculated using FDTD. Lower panel: Zoomed-in view of the low intensity ANAuNP (blue) and NCAuNR (green) spectra.

Far-Field Optical Response and Near-Field SERS Relationship

The LSPR band observed at ~550 nm in the far-field spectra of IFAuNP and ANAuNP (Figure 2) originates from AuNP monomers, which, as was previously shown, do not contribute to the near-field enhancement.[53] AuNP dimers, trimers, and their higher order clusters exhibit a broad LSPR band at 700–800 nm (Figures 2 and 5). Dense AuNR aggregates of NCAuNR result in the formation of a very broad LSPR band centered ~1 μm (Figure 5 and Supporting Information, Figure S3). Using WS-SERES and FDTD we have demonstrated that AuNP and AuNR aggregates primarily govern the near-field SERS responses of 3D SERS substrates. Moreover, the LSPR bands of AuNP and AuNR aggregates almost perfectly overlap with the maxima of the near-field surface-enhanced Raman scattering response of the corresponding 3D SERS substrates. Previously, the relationship between far-field spectroscopic properties and near-field surface-enhanced Raman scattering has been determined for 2D SERS substrates, known as nanorod arrays.[16, 51] It was shown that periodic nanorod arrays showed a red-shift (~150 nm) of their near-field SERS response with respect to the LSPR.[16] Therefore, we can conclude that 3D SERS substrates

have a substantially different relationship between far-field optical response and near-field surface-enhanced Raman scattering than previously reported 2D SERS substrates.

Estimation of Enhancement Factor for 3D SERS Substrates

Successful detection and identification of various analytes directly depends on the substrate enhancement factor (EF). Enhancements in the range 10^4–10^8 are commonly reported for both lithographic and non-lithographic SERS substrates, as well as nanoparticle and nanorod assemblies.[25] A direct determination of the EF for the 3D SERS substrates is extremely challenging due to the difficulty to define the area of Au surface illuminated by the laser excitation, and to determine the beam penetration depth within the substrate. This consequently does not allow identifying the number of molecules actually contributing to the SERS signal. Therefore, to estimate the EF of these 3D SERS substrates we used previously reported non-lithographic SERS substrates, known as film over nanospheres (FONs). Since the IFAuNP and ANAuNP substrates exhibited optimal SERS efficiency at ~785 nm we have optimized the FON to give a comparable SERS efficiency (100 arb. u.) at ~785 nm and then calculated the EF at this wavelength (Figure S4). Since the number of benzenethiol molecules contributing to the calculations of the SERS enhancement can be defined for FON SERS substrates, we were able to calculate the EF. The EF was calculated to be 10^7. This appears to be in good agreement with EF~10^8 predicted by the FDTD simulations (Figure 4D–F). It should be noted that the obtained EF value for the FON substrates cannot be directly extrapolated to the 3D SERS substrates because of the uncertainties previously discussed. Nevertheless, it provides an order of magnitude of the SERS enhancement, which is expected to be achieved on the IFAuNP and ANAuNP 3D SERS substrates and, consequently, 100 times lower on the NCAuNR substrate at 785 nm laser excitation.

Conclusions

Using a comprehensive spectroscopic approach, coupled with finite-difference time-domain simulations, we investigated the near- and far-field relationship in several commercial (IFAuNP and ANAuNP) and non-commercial (NCAuNR) 3D SERS substrates. The LSPR profiles obtained for the IFAuNP, ANAuNP, and NCAuNR substrates were distinct from previously reported non-lithographic SERS substrates.[11, 16, 51, 56] It was found that far-field spectroscopic properties of IFAuNP and ANAuNP were primarily determined by AuNPs monomers. NCAuNR exhibited no clearly defined LSPR bands. This condition leads to a troublesome experimental problem in profiling and understanding the LSPR modes of the 3D SERS substrates. Therefore, we have used wavelength scanned surface-enhanced Raman excitation spectroscopy (WS-SERES) to investigate the near-field surface-enhanced Raman scattering properties of the 3D SERS substrates. Based on the experimental near-field responses of the 3D SERS substrates, their microscopic investigation, and FDTD calculations we have predicted their LSPR far-field profiles. We have found that near-filed properties of 3D SERS substrates are primarily determined by nanoparticle dimers, trimers, and higher order nanoparticle clusters. LSPR bands of these nanoparticle aggregates near perfectly overlap with the maxima of the near-field surface-enhanced Raman scattering responses of the 3D SERS substrates. This allowed us to determine the relationship between far-field optical response and near-field surface-enhanced Raman scattering of these 3D SERS substrates.

Acknowledgements

The authors thank Dr. John Rabolt from the University of Delaware, Newark, for the fabrication of the AuNR substrates and thank iFyber and Diagnostic AnSERS for generously providing the AuNP substrates and the absorption spectra of the colloidal nanoparticles. This research was supported by the Northwestern Materials Research Center under NSF grant DMR-1121262 and U.S. Army SBIR grant, award W911NF-13-C-0051. This work made use of the EPIC facility (NUANCE Center-Northwestern University), which has received support from the MRSEC program (NSF DMR-1121262) at the Materials Research Center; the International Institute for Nanotechnology (IIN); and the State of Illinois, through the IIN.

References

1 R. P. Van Duyne and D. L. Jeanmaire, *J. Electroanal. Chem.*, 1977, **84**, 1-20.
2 S. L. Kleinman, R. R. Frontiera, A. I. Henry, J. A. Dieringer and R. P. Van Duyne, *Phys. Chem. Chem. Phys.*, 2013, **15**, 21-36.
3 B. Sharma, R. R. Frontiera, A. I. Henry, E. Ringe and R. P. Van Duyne, *Mater. Today*, 2012, **15**, 16-25.
4 R. J. Brown and M. J. T. Milton, *J. Raman. Spectr.*, 2008, **39**, 1313-1326
5 M. Moskovits, *J. Chem. Phys.*, 1978, **69**, 4159-4161.
6 J. Gersten and A. Nitzan, *J. Chem. Phys.*, 1980, **73**, 3023-3037.
7 M. Kerker, D. S. Wang and H. Chew, *Appl. Opt.*, 1980, **19**, 3373-3388.
8 F. W. King, R. P. Van Duyne and G. C. Schatz, *J. Chem. Phys.*, 1978, **69**, 4472-4481.
9 K. L. Kelly, E. Coronado, L. L. Zhao and G. C. Schatz, *J. Phys. Chem. B*, 2003, **107**, 668-677.
10 K. L. Wustholz, A. I. Henry, J. M. McMahon, R. G. Freeman, N. Valley, M. E. Piotti, M. J. Natan, G. C. Schatz and R. P. Van Duyne, *J. Am. Chem. Soc.*, 2011, **132**, 10903-10910.
11 A. J. Haes, C. L. Haynes, A. D. McFarland, G. C. Schatz, R. P. Van Duyne and S. Zou, *MRS Bull.*, 2005, **30**, 368-375.
12 E. Ringe, J. M. McMahon, K. Sohn, C. Cobley, Y. Xia, J. Huang, G. C. Schatz, L. D. Marks and R. P. Van Duyne, *J. Phys. Chem. C*, 2010, **114**, 12511-12516.
13 J. P. Camden, J. A. Dieringer, J. Zhao and R. P. Van Duyne, *Acc. Chem. Res.*, 2008, **41**, 1653-1661.

14 L. A. Dick, A. D. McFarland, C. L. Haynes and R. P. Van Duyne, *J. Phys. Chem. B*, 2002, **106**, 853-860.

15 D. M. Kuncicky, B. G. Prevo and O. D. Velev, *J. Mater. Chem.*, 2006, **16**, 1207-1211.

16 M. D. Doherty, A. Murphy, J. McPhillips, R. J. Pollard and P. Dawson, *J. Phys. Chem. C.*, 2010, **114**, 19913-19919.

17 C. L. Haynes, A. D. McFarland, L. L. Zhao, R. P. Van Duyne, G. C. Schatz, L. Gunnarsson, J. Prikulis, B. Kasemo and M. Kall, *J. Phys. Chem. B*, 2003, **107**, 7337-7342.

18 M. A. De Jesus, K. S. Giesfeldt, J. M. Oran, N. A. Abu-Hatab, N. V. Lavrik and M. J. Sepaniak, *Appl. Spectrosc.*, 2005, **59**, 1501-1508.

19 S. Bernard, N. Felidj, S. Truong, P. Peretti, G. Levi and J. Aubard, *Biopolymers*, 2002, **67**, 314-318.

20 Q. Yu, P. Guan, D. Qin, G. Golden and P. M. Wallace, *Nano Lett.*, 2008, **8**, 1923-1928.

21 Q. Zhang, N. Large, P. Nordlander and H. Wang, *J. Phys. Chem. Lett.*, 2014, **5**, 370-374.

22 Q. Zhang, N. Large and H. Wang, *Appl. Mater. Interfaces*, 2014, **6**, 17255-17267.

23 H. Jing, Q. Zhang, N. Large, C. Yu, D. A. Blom, P. Nordlander and H. Wang, *Nano Lett.*, 2014, **14**, 3674-3682.

24 P. L. Stiles, J. A. Dieringer, N. C. Shah and R. P. Van Duyne, *Ann. Rev. Anal. Chem.*, 2008, **1**, 601-626.

25 N. G. Greeneltch, M. G. Blaber, A. I. Henry, G. C. Schatz and R. P. Van Duyne, *Anal. Chem.*, 2013, **85**, 2297-2303.

26 E. J. Gunnarsson, H. Bjerneld, S. Xu, B. Petronis, B. Kasemo and M. Kall, *Appl. Phys. Lett.*, 2001, **78**, 802-804.

27 T. Atay, J.-H. Song and A. V. Nurmikko, *Nano Lett.*, 2004, **2004**, 1627-1631.

28 J. A. Dieringer, A. D. McFarland, N. C. Shah, D. A. Stuart, A. V. Whitney, C. R. Yonzon, M. A. Young, X. Zhang and R. P. Van Duyne, *Farad. Discuss.*, 2006, **132**, 9-26.

29 P. F. Liao, J. G. Bergman, D. S. Chemla, A. Wokaun, J. Melngailis, A. M. Hawryluk and N. P. Economou, *Chem. Phys. Lett.* , 1981, **82**, 355-359.

30 C. Y. Chen and E. Burstein, *Phys. Rev. Lett.*, 1980, **45**, 1287-1291.

31 J. F. Betz, W. W. Yu, Y. Cheng, I. M. White and G. W. Rubloff, *Phys. Chem. Chem. Phys.*, 2014, **16**, 2224-2239.

32 E. Ringe, J. Zhang, M. R. Langille, C. A. Mirkin, L. D. Marks and R. P. Van Duyne, *Nanotechnology*, 2012, **23**, 444005.

33 M. J. Mulvihill, X. Y. Ling, J. Henzie and P. Yang, *J. Am. Chem. Soc.*, **132**, 268-274.

34 M. Rycenga, M. R. Langille, M. L. Personick, T. Ozel and C. A. Mirkin, *Nano Lett.*, **12**, 6218-6222.

35 Z. Shao, W. Zhu, H. Wang, Q. Yang, S. Yang, X. Liu and G. Wang, *J. Phys. Chem. C*, 2013, **117**, 14289-14294.

36 D. Kurouski and R. P. Van Duyne, *Anal. Chem.*, 2015, **87**, 2901-2906.

37 H. Wang, C. S. Levin, N. J. Halas, *J. Am. Chem. Soc.*, 2005, **127**, 14992-14993.

38 D. Graham, D. G. Thompson, W. E. Smith and K. Faulds, *Nature Nanotech.*, 2008, **3**, 548-551.

39 R. W. Taylor, T. C. Lee, O. A. Scherman, R. Esteban, J. Aizpurua, F. M. Huang, J. J. Baumberg and S. Mahajan, *ACS Nano*, 2011, **5**, 3878-3887.

40 R. A. Alvarez-Puebla, R. Contreras-Caceres, I. Pastoriza-Santos, J. Perez-Juste and L. M. Liz-Marzan, *Angew. Chem. Int. Ed.* 2009, **48**, 138-143.

41 C. D. Tran, *Anal. Chem.*, 1984, **56**, 824-826.

42 T. Vo-Dinh, M. Uziel and A. L. Morrison, *Appl. Spectr.*, 1987, **41**, 605-610.

43 A. Berthod, J. J. Lasernas and J. D. Winefordner, *J. Pharmaceutical. Biomed. Anal.*, 1988, **6**, 599-608.

44 W. W. Yu and I. M. White, *Analyst*, 2013, **138**, 1020-1025.

45 W. W. Yu and I. M. White, *Anal. Chem.*, **82**, 9626-9630.

46 W. W. Yu and I. M. White, *Analyst*, 2012, **137**, 1168-1173.

47 P. Fierro-Mercado, B. Renteria-Beleno and S. P. Hernandez-Rivera, *Chem. Phys. Lett.*, 2012, **552**, 108-113.

48 E. P. Hoppmann, W. W. Yu and I. M. White, *Methods*, 2013, **63**, 219-224.

49 W.-J. Liao, P. K. Roy and C. Chattopadhyay, *Analyst*, 2014, **4**, 40487-40493.

50 E. P. Hoppmann, W. W. Yu and I. M. White, *J. Select. Topics Quantum Electron.*, 2014, **20**, 7300510.

51 A. D. McFarland, M. A. Young, J. A. Dieringer and R. P. Van Duyne, *J. Phys. Chem. C*, 2005, **109**, 11279-11285.

52 W. Tang, D. B. Chase and J. F. Rabolt, *Anal. Chem.*, 2013, **85**, 10702-10709.

53 K. L. Wustholz, A. I. Henry, J. M. McMahon, R. G. Freeman, N. Valley, M. E. Piotti, M. J. Natan, G. C. Schatz and R. P. Van Duyne, *J. Am. Chem. Soc.*, 2010, **132**, 10903-10910.

54 C. Caro, P. M. Castillo, R. Klippstein, D. Pozo and A. P. Zaderenko, in *Silver Nanoparticles*, ed. D. P. Perez, InTech, 2010, p. 342.

55 A. J. Haes, D. A. Stuart, S. Nie and R. P. Van Duyne, *J. Fluoresc.*, 2004, **14**, 355-367.

56 S. L. Kleinman, B. Sharma, M. G. Blaber, A. I. Henry, N. Valley, R. G. Freeman, M. J. Natan, G. C. Schatz and R. P. Van Duyne, *J. Am. Chem. Soc.*, 2012, **135**, 301-308.

57 Lumerical Solutions, Inc., http://www.lumerical.com/tcad-products/fdtd/.

58 P. B. Johnson and R. W. Christy, *Phys. Rev. B*, 1972, **6**, 4370–4379.

59 N. Sultanova, S. Kasarova and I. Nikolov, *Acta Physica Polonica A*, 2009, **116**, 585-587.

60 C. Douketis, T. L. Haslett, Z. Wang, M. Moskovits and S. Iannotta, *J. Chem. Phys.*, 2000, **113**, 11315–11323.

61 G. C. Schatz and R. P. Van Duyne, in *Handbook of Vibrational Spectroscopy*, eds. J. M. Chalmers and P. R. Griffiths, Wiley, Chichester, 2002, pp. pp. 759–774.

62 D. M. Solís, J. M. Taboada, F. Obelleiro, L. M. Liz-Marzán and F. J. García de Abajo, *ACS Nano*, 2014, **8**, 7559-7570.
63 D. A. G. Bruggeman, *Ann. Phys.*, 1935, **416**, 636-664.
64 J. C. Maxwell Garnett, *Phil. Trans. R. Soc. Lond. A* 1904, **203**, 385-420.
65 J. C. Maxwell Garnett, *Phil. Trans. R. Soc. Lond. A* 1906, **205**, 237-288.